Published in final edited form as:
Mol Cancer Ther. 2009 April ; 8(4): 947–958. doi:10.1158/1535-7163.MCT-08-0981.

The selective hypoxia inducible factor-1 inhibitor PX-478 provides *in vivo* radiosensitization through tumor stromal effects

David L. Schwartz[1,2], **Garth Powis**[3], **Arun Thitai-Kumar**[2], **Yi He**[1], **James Bankson**[4], **Ryan Williams**[3], **Robert Lemos**[3], **Junghwan Oh**[1], **Andrei Volgin**[2], **Suren Soghomonyan**[2], **Ryuichi Nishii**[2], **Mian Alauddin**[2], **Uday Mukhopadhay**[2], **Zhenghong Peng**[3], **William Bornmann**[3], and **Juri Gelovani**[2]

[1]Department of Radiation Oncology, The University of Texas M. D. Anderson Cancer Center, Houston, Texas

[2]Department of Experimental Diagnostic Imaging, The University of Texas M. D. Anderson Cancer Center, Houston, Texas

[3]Department of Experimental Therapeutics, The University of Texas M. D. Anderson Cancer Center, Houston, Texas

[4]Department of Imaging Physics, The University of Texas M. D. Anderson Cancer Center, Houston, Texas

Abstract

Hypoxia inducible factor-1 (HIF-1) promotes tumor cell adaptation to microenvironmental stress. HIF-1 is up-regulated in irradiated tumors and serves as a promising target for radiosensitization. We initially confirmed that the orally bioavailable HIF-1 inhibitor PX-478 reduces HIF-1 protein levels and signaling *in vitro* in a dose-dependent manner and provides direct radiosensitization of hypoxic cancer cells in clonogenic survival assays using C6 glioma, HN5 and UMSCCa10 squamous cells, and Panc-1 pancreatic adenocarcinoma cell lines. However, PX-478 yields striking *in vivo* tumor sensitization to single-dose irradiation, which cannot be explained by incremental improvement in direct tumor cell killing. We show that PX-478 prevents postradiation HIF-1 signaling and abrogates downstream stromal adaptation in C6 and HN5 reporter xenografts as measured by serial ultrasound, vascular magnetic resonance imaging, and hypoxia response element–specific micro–positron emission tomography imaging. The primacy of indirect PX-478 *in vivo* effects was corroborated by our findings that (*a*) either concurrent or early postradiation sequencing of PX-478 provides roughly equivalent sensitization and (*b*) constitutive vascular endothelial growth factor expression maintains refractory tumor vessel function and progression following combined radiation and PX-478. These results confirm that disruption of postradiation adaptive HIF-1 signaling by PX-478 imparts increased therapeutic efficacy through blockade of HIF-1–dependent reconstitution of tumor stromal function. Successful translation of targeted HIF-1 radiosensitization to the clinical setting will require specific consideration of tumor microenvironmental effects and mechanisms.

Requests for reprints: David L. Schwartz, The University of Texas M. D. Anderson Cancer Center, Unit 97, 1515 Holcombe Boulevard, Houston, TX 77030. Phone: 713-563-2341; Fax: 713-563-2331. docdls@mdanderson.org.
Note: D. Schwartz and G. Powis contributed equally to this work.

Disclosure of Potential Conflicts of Interest
G. Powis: owns stock in Oncothyreon, Inc. No other potential conflicts of interest were disclosed.

Introduction

Tumor hypoxia is known to contribute to tumor radioresistance and poor clinical outcomes (1–3). The presence of oxygen during radiation exposure is necessary to achieve generation of free oxygen radicals and DNA damage for tumor killing and is the basis for the so-called "oxygen effect" (4). Tumor cells that survive hypoxic stress are selected for reduced apoptotic potential, increased anaerobic glycolysis, tolerance to extracellular acidity, increased migration, and angiogenic signaling. The biological cornerstone of these hypoxia-specific stress responses is the hypoxia inducible factor (HIF) family of transcription factors (5). HIF-1, the best studied member, is a heterodimer consisting of a tightly regulated HIF-1α subunit and a constitutively expressed HIF-1β subunit. Low oxygen levels enhance HIF-1 expression through increased protein stability (6), leading to downstream expression of genes affecting angiogenesis, glycolysis, apoptosis, differentiation, and proliferation.

Targeted inhibition of HIF-1 signaling has generated interest for inhibiting tumor growth (7) and overcoming resistance to radiation and chemotherapy (8). Targeted HIF-1 blockade would be expected to provide a broader efficacy than inhibition of downstream effectors such as vascular endothelial growth factor (VEGF), with fewer available pathways of resistance (9). Selective HIF-1 inhibitors are entering early clinical testing (7,10). PX-478 (S-2-amino-3-[4′-*N*,*N*,-bis(chloroethyl)amino]phenyl propionic acid N-oxide dihydrochloride) is a novel agent that suppresses constitutive and hypoxia-induced HIF-1 in cancer cell lines by inhibiting HIF-1 translation (11). PX-478 shows promising activity against human tumor xenografts (12,13) and is unique among HIF-1 inhibitors undergoing clinical evaluation in that it is orally bioavailable (10).

We investigated the mechanisms and efficacy of PX-478 radiosensitization *in vitro* and *in vivo*. We confirmed that PX-478 inhibits HIF-1 signaling in a dose-dependent manner and provides direct radiosensitization in hypoxic conditions. The therapeutic efficacy of PX-478 improves markedly *in vivo*, where it provides durable inhibition of tumor growth following single-fraction radiation. This seems to be achieved less through autonomous cancer cell effects than through blockade of HIF-1–dependent angiogenic tumor adaptation to radiation. Serial ultrasound, vascular magnetic resonance imaging (MRI), and positron emission tomography (PET) detection of HIF-1 tumor signaling confirm inhibition of postradiation HIF-1–mediated recovery of tumor stromal function with PX-478. PX-478 does not require concurrent sequencing with radiation and can provide durable growth inhibition if given sequentially after irradiation. Constitutive VEGF expression restores refractory tumor progression following combined radiation and PX-478. Together, our data support a mechanistic model in which tumor radioresistance is predominantly mediated by tumor-stromal interactions and by the capacity of tumor to compensate for radiation-induced vascular damage through ischemic HIF-1–dependent angiogenic signaling. Inhibition of postradiation HIF-1 signaling with PX-478 is a promising strategy to disrupt this adaptive cascade and to overcome tumor radioresistance.

Materials and Methods

Cell Lines

Rat C6 glioma and human Panc-1 pancreatic adenocarcinoma cell lines were obtained from the American Type Culture Collection, whereas human HN5 and UMSCCA10 head and neck squamous carcinoma cell lines were obtained from Dr. Luka Milas (The University of Texas M. D. Anderson Cancer Center). C6 and HN5 HIF-1 reporter cells were stably transfected with a bifunctional reporter consisting of herpes simplex virus 1-thymidine kinase (HSV-tk) and green fluorescent protein (GFP) under transcriptional control of the hypoxia response element (HRE-tk/eGFP-cmvRed 2XPRT) as described previously (14,15).

This construct generates intranuclear GFP signal and HSV-tk retention of the radiolabeled gancyclovir analogue 2′-^{18}F-fluoro-2′-deoxy-5-ethyl-1-β-D-arabionofuranosyluracil (^{18}F-FEAU), allowing *in vivo* PET imaging of tumor cell HIF-1 signal. C6 cells constitutively expressing murine VEGF (C6-V) were generated via stable transfection with a pBLAST49-mVEGF v21 plasmid (InvivoGen) using Lipofectamine 2000 per manufacturer's protocol. C6 cells transfected with empty parental plasmid were created as controls. Transfected C6-V cells were initially selected with Blasticidin S (10 μg/mL) and subsequently selected for expression of secreted VEGF and hypoxia-stimulated GFP signal.

Hypoxia Assays

For experiments in hypoxic conditions, culture flasks and plates were incubated for noted times and sequences at 37°C in humidified hypoxic air (1% O_2, 5% CO_2, 94% N_2) using an InVivo Hypoxic Workstation 400 with a Ruskin hypoxic gas mixer (Biotrace International).

Western Blotting

Western blotting for nuclear HIF-1 protein was done as described previously (11). Blots were quantified using ImageQuant software (GE Healthcare), using actin as a loading control. Nuclear extracts were prepared using NE-PER Nuclear and Cytoplasmic Extraction Reagents (Pierce Biotechnology).

Soluble VEGF ELISA Quantification

HN5 and UMSCCA10 cells were plated in triplicate onto 6-cm dishes and cultured with DMEM serum-free medium. After specified treatments, cell culture media were collected. The media were further diluted, and secreted VEGF165 and VEGF 121 protein isoform levels per milligram of total secreted protein were quantified by an ELISA kit (R&D System), according to the manufacturer's protocol.

PX-478 Dose Response Determination

C6 HIF-1 reporter cells in log phase growth were distributed into 96-well plates at 3×10^3 cells/50 μL. For normoxic conditions, cells were grown overnight and then treated with PX-478 at 0.1 to 200 μmol/L, with or without concurrent 150 μmol/L $CoCl_2$ for 24 h. Experiments were repeated in hypoxic conditions, with C6 HIF-1 reporter cells incubated at 1% O_2 for 24 h and then treated with PX-478 at equivalent concentrations for 24 h. HIF-1–dependent GFP signal normalized to beacon RFP signal was determined by fluorescence spectrometry via an automated TECAN Freedom Evo microplate reader. Cells were assayed in quadruplicate wells. Cell viability was confirmed via 4-h WST-1 metabolism (Clontech). EC_{50} graph plotting was done with GraphPad Prism v.4.

Clonogenic Survival Assays

C6, HN5, Panc-1, and UMSCCA10 cells were grown to 70% confluence and incubated at 21% O_2 (normoxia) or 1% O_2 (hypoxia, via chamber) for 24 h. Cells were treated with 25 μmol/L PX-478 for 24 h and irradiated with a ^{137}Cs source (5.8 Gy/min), with atmospheric conditions maintained. Cells were assayed for colony formation by replating at specified numbers into six-well plates in a drug-free medium. The cells were immediately plated after irradiation, maintained for 12 d in normoxia, and stained with 0.5% crystal violet in absolute ethanol. Colonies with >50 cells were counted. Clonogenic survival curves were constructed from at least three independent experiments.

In vivo Tumor Xenografting and Antitumor Studies

C6 or HN5 cells (2×10^6) were implanted s.c. into *nu/nu* mice. Xenografts grew to 100 to 150 mm^3 over 2 wk. Tumor volumes were calculated by digital calipers as π/6 [(short axis in

mm)^2 × (long axis in mm)]. Animals were handled according to the Institutional Animal Care and Utilization Committee guidelines. Mice were stratified into groups of 8 to 10 animals having equal mean tumor volumes. When tumors reached ≥2,000 mm^3 or became necrotic, animals were euthanized.

Animal Irradiation/PX-478 Treatment

Irradiated tumors received 8 Gy radiation via ^{60}Co unit (1.8 Gy/min) with custom shielding. PX-478 was synthesized in The University of Texas M. D. Anderson Cancer Center Department of Experimental Therapeutics and delivered via p.o. gavage at 30 mg/kg × 2 consecutive days. Untreated control xenografts underwent mock irradiation.

Immunohistochemical Staining and Analysis

Pimonidazole (25 mg/mL) was injected i.v. 60 min before sacrifice. Tumors were fixed in 4% formaldehyde/PBS and processed into paraffin and sectioned at 4-μm thickness. Four tumors for each treatment condition were collected, bisected, and then serially sectioned (10 adjacent sections, 5 μm thickness) at 100- to 150-μm intervals in either direction. Immunohistochemical staining was done on a Vision Biosystems Bondmax automated slide stainer (VBS). Nuclei were visualized by hematoxylin. GFP and VEGF were detected by using rabbit polyclonal antibodies from Abcam and R&D Systems, respectively. Pimonidazole adducts were stained using a FITC-labeled monoclonal antibody, followed by a horseradish peroxidase–conjugated anti-FITC polyclonal antibody (Hypoxyprobe-1 Plus, Chemicon). Specificity of staining was evaluated via nonspecific control antibodies. Images were acquired using a Nikon e90i microscope with automated stage and a Roper Coolsnap K4 digital camera (Roper Scientific) through a plan-apo 4× objective. Sections were imaged in their entirety and quantitatively analyzed using Compix SimplePCI (Compix, Inc.) software.

MicroPET Whole Animal Imaging

^{18}F-FEAU was synthesized using a modified no-carrier added procedure (16). For each time point and study condition, 6 to 10 mice were injected (i.v.) with 100 μCi (100 μL) of ^{18}F-FEAU. Fifteen-minute static images were acquired under inhalation anesthesia using a microPET scanner (Concorde Microsystems, R4). Images were reconstructed by using ordered subset expectation maximization algorithm. Regional radioactivity concentrations (kBq/cm^3 or μCi/cm^3) for ^{18}F-FEAU was estimated from regions of interest drawn around the tumor or organ on trans-axial slices of the reconstructed image sets. The radioactivity uptake in tumor (kBq/cm^3 or μCi/cm^3) was converted to percent injected dose per gram (% ID/g). Tumor tracer uptake was normalized to background muscle uptake and quantified as a maximal tumor-to-muscle ratio (TMR) averaged from three separate levels on axial projection, measured in triplicate with standardized 3- to 7-pixel diameter two-di mensional regions of interest.

Ultrasound Imaging

Ultrasound imaging of xenografts was done with a Vevo 770 unit (VisualSonics), using a single-element transducer with 40-MHz center frequency. Power Doppler settings were held constant at 25-dB Power Doppler gain, 5-kHz pulse repetition rate, and 2.5 mm/s wall filter with 2 mm/s scan speed. Initial imaging of tumor was done in B-mode to discriminate tumor boundaries, and Doppler images were acquired for a manually delineated region of interest encompassing the entire tumor. Vascular area in tumor was calculated by color pixel density, defined as the ratio of the number of color pixels to total number of pixels within the region of interest.

MRI Imaging

Serial dynamic, contrast-enhanced (DCE)-MRI was acquired using a 4.7-T Biospec USR47/40 (Bruker Biospin MRI, Inc.) with a 35-mm linear volume resonator and 60-mm micro-imaging gradients. A three-plane rapid acquisition relaxation enhanced imaging sequence was used to confirm animal positioning, and coronal T_2-weighted rapid acquisition relaxation enhanced images (TE/TR 70/4,000 ms, FOV 4 cm × 3 cm, matrix 256 × 192, rapid acquisition relaxation enhanced factor 12) were used for tumor localization. Axial T_1-weighted spin-echo images (TE/TR 8.5 ms/700 ms, FOV 4 cm × 3 cm, matrix 256 × 192) were acquired before and after administration of 0.2 mL/kg gadopentetate dimeglumine (Gd-DTPA: Magnevist, Berlex Laboratories). DCE-MRI data were acquired using a multislice fast spoiled gradient-recalled echo sequence (TE/TR 1.4/40 ms, FOV4 cm × 3 cm, matrix 128 × 96, 35 excitation angle, 3.8 s/repetition, 100 repetitions). Baseline images were collected for 1 min before injection of the contrast agent. A generalized kinetic model was applied to manually segmented data using Matlab (The Mathworks).

Statistical Testing

The significance of differences between pooled results from indicated study groups was tested via the Student's *t* test or one-way ANOVA with GraphPad Prism v.4.

Results

PX-478 Inhibits HIF-1 Signaling in a Dose-Dependent Manner

Western blotting confirmed dose-dependent reductions of nuclear HIF-1 protein levels in hypoxia-stimulated HN5 and UMSCCA10 cells (Fig. 1A). PX-478 inhibited the activity of a HIF-1–dependent GFP reporter construct transfected into C6 cells exposed to chemical hypoxia (150 μmol/L $CoCl_2$, 24 hours) or moderate physical hypoxia (1% O_2, 24 hours; Fig. 1B), with an IC_{50} value of 49.2 μmol/L. Twenty-five micromoles per liter of PX-478 inhibited expression of soluble VEGF, a downstream protein regulated by HIF-1, in hypoxic HN5 and UMSCCa10 cells (110 pg/mg total protein versus 255 pg/mg in untreated HN5 cells, $P < 0.001$; 121 pg/mg versus 242 pg/mg in untreated UMSCCa10 cells, $P < 0.001$; Fig. 1C). PX-478 did not affect baseline VEGF secretion in normoxic cells.

PX-478 Provides Direct Radiosensitization *In vitro*

Clonogenic survival assays done with C6, HN5, UMSCCa10, and Panc-1 cells show direct radiosensitization of hypoxic cells (1% O_2) treated 24 hours before radiation with 25 μmol/L PX-478 (Fig. 2). PX-478 treatment elicited minimal sensitization of normoxic cells. PX-478 provided consistent hypoxic radiosensitization across all cell lines [for C6, a SF2 (enhancement factor at 0.2 surviving fraction) of 1.42 versus 1.06 was shown in 1% and 21% O_2 conditions, respectively; for HN5, 1.37 versus 1.08; for UMSCCa10, 1.40 versus 1.07; and for Panc-1, 1.42 versus 1.05).

PX-478 Inhibits Adaptive Postradiation Tumor HIF-1 Signaling *In vivo* and Provides Durable Enhancement of Radiation Growth Delay

Using C6 HIF-1 reporter cells, we characterized postradiotherapy tumor HIF-1 signaling via serial *in situ* ^{18}F-FEAU-PET imaging of *nu/nu* mouse cohorts ($n = 10$) over 8 days. Radiation at 8 Gy induced delayed up-regulation of HIF-1 activity in C6 reporter cells at 48 hours [mean TMR of ^{18}F-FEAU accumulation = 4.51 ± 0.23 (SE) versus 3.97 ± 0.11 for controls, $P < 0.05$) and peaked by day 6 posttreatment (mean maximum TMR = 7.85 ± 0.24 versus 5.77 ± 0.18 for controls, $P < 0.005$). Timing of HIF-1 up-regulation at 48 hours was corroborated by serial immunohistochemical staining of tumor tissue (Fig. 3). HIF-1 up-regulation was heterogeneous and tightly localized to discrete viable regions within tumors.

HIF-1 activity normalized by day 8 to levels seen in controls (mean maximum TMR = 5.64 ± 0.22 versus 5.21 ± 0.17 for controls, P = n.s.), indicating reconstitution of tumor microenvironmental conditions. Identical findings were seen in a HN5 reporter xenograft model (n = 6). HIF-1 up-regulation was accompanied by delayed yet uninterrupted tumor growth. These findings suggest that *in vivo* cancer radioresistance is closely associated with the ability of vascularized tumors to generate compensatory HIF-1–dependent stromal revascularization and subsequent resolution of ischemia. We therefore hypothesized that HIF-1 inhibition with PX-478 would provide superior radiosensitization *in vivo* than what was suggested by our *in vitro* assays.

We next confirmed *in vivo* PX-478 activity via ^{18}F-FEAU-PET imaging of tumor HIF-1 signal activity. We treated *nu/nu* mice with C6 or HN5 reporter xenografts with 30 mg/kg p.o. PX-478 for 2 consecutive days. PX-478 prevented the expected appearance of HIF-1 transcriptional activity in central ischemic regions of C6 tumors (n = 8–10, mean maximum TMR = 1.83 ± 0.87 SD at day 2, versus 3.97 ± 0.41 in untreated tumors, $P < 0.01$; Fig. 3A). By day 4 after PX-478 treatment, there was reemergence of HIF-1 signaling and tumor growth. A significant increase in mean maximum TMR was seen by day 8 (5.23 ± 0.83 versus 1.86 ± 0.44 at baseline, $P < 0.001$). Similar findings were confirmed in HN5 reporter xenograft tumors (n = 6), although these cells seemed more resistant to single-agent treatment. A brief rebound in HIF-1 signal was seen after drug release, accompanied by an acceleration of tumor growth, which ended by day 6. Subsequent experiments confirmed continued albeit slow HN5 xenograft growth past this time point.

Treatment (8 Gy) of C6 reporter xenografts given 4 hours after a 2-day course of 30 mg/kg PX-478 durably inhibited HIF-1 transcriptional activity (mean maximum TMR = 1.35 ± 0.09 at day 8 postradiation, versus 1.97 ± 0.10 at baseline, $P < 0.001$; Fig. 3A). This was corroborated by quantified immunohistochemical staining of C6 tissue (n = 4 tumors × 5 tissue sections) for HIF-1–dependent GFP and downstream VEGF expression (Fig. 3B). Importantly, tumor growth ceased over the 8-day posttreatment time course. Identical findings were observed in HN5 xenografts (Fig. 3C). This emphasizes not only the central role of HIF-1 in tumor growth recovery but also suggests that PX-478 tumor radiosensitization is mediated not through a direct effect on tumor cells but through interruption of downstream tumor stromal adaptation.

In situ Imaging Shows Durable Inhibition of Posttreatment Tumor Stromal Recovery in C6 Tumor Xenografts following Combined PX-478 and Radiation

Irradiation (8 Gy) alone or a 2-day course of 30 mg/kg PX-478 led to transient disruption of tumor blood flow on power Doppler ultrasound (n = 6 per cohort). This was observed within 24 hours following completion of radiation (74.9% ± 1.1% decrease, $P < 0.001$) or PX-478 (62.6 ± 5.7% decrease, $P < 0.001$). Tumor vessel flow returned toward baseline at 48 hours, consistent with early vascular adaptation downstream of HIF-1 signaling. In contrast, ultrasound confirmed durable disruption of tumor vessel flow in C6 xenografts at 7 days following concurrent (day before and day of radiation) 30 mg/kg PX-478 and 8 Gy (44.7% ± 2.8% decrease from baseline, $P < 0.005$; Fig. 4A). Serial DCE-MRI K_{trans} mapping with small molecular weight Gd-DTPA (n = 5 per cohort) showed acutely increased tumor K_{trans} values (578% ± 57% increase, $P < 0.05$) within 24 hours following radiation (Fig. 4B), consistent with increased tumor vessel permeability. Tumor K_{trans} measurements subsequently normalized by 7 days posttreatment. Single-agent PX-478 treatment has previously been confirmed by DCE-MRI to transiently reduce tumor K_{trans} 24 hours after administration (13). Concurrent treatment with 30 mg/kg PX-478 and radiation abrogated postradiotherapy VEGF signaling (Fig. 3B) and postradiation increases in tumor K_{trans} (Fig. 4B). Thus, inhibition of early adaptive HIF-1 signaling events by PX-478 following

irradiation disables supportive proangiogenic signaling and durably blocks tumor vessel recovery.

In vivo PX-478 Radiosensitization Is Mediated by Effects on Angiogenic Stromal Adaptation to Radiation

To determine the importance of direct PX-478 tumor cell sensitization at the time of irradiation, we next investigated whether concurrent administration with radiation was required for PX-478 *in vivo* efficacy. We treated *nu/nu* mice bearing C6 ($n = 8$) and HN5 ($n = 10$) xenograft cohorts with a 2-day course of 30 mg/kg p.o. PX-478 either concurrently (given the day before and day of radiation) or adjuvantly (initiated the day following irradiation) with 8 Gy. Both tumor types displayed varying degrees of *in vivo* sensitivity to single-agent PX-478, with HN5 tumors being more resistant to drug relative to radiation. Nonetheless, concurrent and sequential PX-478 provided additive sensitization out to Days 8 to 14 (Fig. 5A). Quantitative immunohistochemical staining of C6 tumors confirmed that early administration of PX-478 with radiation inhibited adaptive HIF-1 and VEGF signaling throughout the 8-day time course (Fig. 5B). Inhibition of HIF-1 and VEGF signaling was less durable following sequential sequencing. Nonetheless, adjuvant PX-478 inhibited the expected peak of ischemic HIF-1 and VEGF signaling 48 hours following radiation and inhibited tumor growth.

To directly confirm the significance of PX-478 tumor stromal effects relative to tumor cell radiosensitization, C6 cells were stably transfected with a constitutive murine VEGF construct (C6-V) to provide uninterrupted proangiogenic signaling to host mouse stroma following radiation independent of HIF-1 status. Baseline *in vitro* experiments in C6-V monolayers cultured in 1% O_2 confirmed that VEGF secretion was not altered following 8 Gy treatment (Fig. 6A); in addition, *in vitro* radiation clonogenic survival curves were unchanged in C6-V cells relative to control C6 cells or C6 cells transfected with empty parental vector, and treatment with doses of up to 50 μmol/L PX-478 did not significantly inhibit elevated levels of secreted protein in hypoxic C6-V cells (data not shown). On DCE-MRI mapping, C6-V xenografts ($n = 5$) showed a higher baseline K_{trans} than control C6 cells (0.81 ± 0.05 versus 0.42 ± 0.06, $P < 0.001$; Fig. 6B), consistent with VEGF effects on vessel permeability. Unlike control cells, delayed partial reconstitution of refractory growth was observed by day 7 in C6-V xenografts ($n = 6$ per cohort) treated with either 8 Gy alone or with concurrent (day before and day of radiation) 30 mg/kg p.o. PX-478 and 8 Gy. Also, stable, elevated C6-V tumor K_{trans} values were observed after either of these treatments, consistent with continued VEGF angiogenic signaling and downstream tumor vessel permeability effects. These data show the principal mechanism for PX-478 radiosensitization *in vivo* in C6 xenografts to be inhibition of HIF-1–dependent proangiogenic signaling, in part mediated by VEGF.

Discussion

Hypoxia increases the resistance of cancer to radiation treatment (1–3,17). Within intact tumors, the dynamics and biological effects of hypoxia are determined by the presence of distinct tumor and host stromal cell populations that interact to adapt to microenvironmental stress (18). Tumor cells that successfully adapt to stressful environmental conditions are able to co-opt and then induce stromal blood vessels to enhance their oxygen and nutrient supply by paracrine growth factor signaling. HIF-1–stimulated proangiogenic tumor cell signaling, such as VEGF expression, is important to this process (9).

In this current study, we determined that PX-478 provides inhibition of HIF-1 expression and varying degrees of direct tumor cell radiosensitization across a spectrum of cell lines (Figs. 1 and 2). We went on to show that PX-478 yields more striking radiosensitization to

single-dose irradiation *in vivo*, greater than what would be expected from an incremental increase in direct tumor cell killing (Fig. 3).We subsequently confirmed that PX-478 acts to inhibit postradiation recovery *in vivo* through inhibition of HIF-1–dependent stromal reconstitution (Figs. 4 and 5), which can be partially overcome by constitutive downstream VEGF angiogenic signaling (Fig. 6). Our observed effects of PX-478 on tumor stroma are consistent with a broad blockade of downstream proangiogenic pathways responsible for HIF-1–mediated tumor stress responses and are potentially less vulnerable to parallel adaptive pathways that limit the efficacy of agents targeted to specific downstream proangiogenic proteins, such as VEGF.

PX-478 has previously been confirmed by vascular MRI imaging to strongly affect tumor vessel physiology *in vivo* (13). The results of single-tracer DCE-MRI imaging depend acutely on the contrast agent chosen. K_{trans} determined by macromolecular contrast agents are value limited by the vessel permeability surface area product rather than input blood flow, whereas results with clinically available low molecular weight Gd-DTPA (as used in the current study) depend on both permeability and flow. Previous DCE-MRI with bovine serum albumin–conjugated Gd-DTPA showed that single-dose PX-478 causes an acute decrease in tumor vessel permeability surface area product in HT-29 cells, which can be seen for at least 24 hours (13). This paralleled the results seen following treatment with the anti-VEGF monoclonal antibody bevacizumab, indicating downstream antiangiogenic activity with PX-478. Available data for preclinical DCE-MRI characterization of acute radiation tumor effects does not provide consensus characterization of early posttreatment stromal effects on account of use of varying radiation treatment schemas, contrast agents, and tumor models. Studies using high molecular weight contrast agents (19–21) showed early incremental decreases in vessel permeability following fractionated radiation treatment. Kobayashi and colleagues (20), showed an increase in K_{trans} with macromolecular contrast enhanced MRI 24 hours following a high-dose (15 Gy) signal fraction treatment. We chose a more moderate single dose (8 Gy) to facilitate the study of acute tumor cell–dependent stromal effects while limiting direct endothelial toxicity. Our complementary use of high-frequency ultrasound measurement of tumor blood flow together with small molecular weight DCE-MRI shows that radiation yields an acute increase in K_{trans} by 24 hours in C6 xenografts (Fig. 4B), which accompanies an acute decrease in tumor blood flow and precedes ischemic HIF-1 tumor cell signaling detected at 48 hours. Concurrent HIF-1 blockade with PX-478 completely abrogated postradiotherapy VEGF signaling and posttreatment changes in K_{trans}, leading to durable inhibition of postradiotherapy tumor vessel function recovery by day 7 (Fig. 4). This finding indicates that small molecular weight contrast DCE-MRI detection of increased tumor vessel permeability following intermediate dose irradiation is driven strongly by the vascular effects of adaptive tumor VEGF up-regulation rather than direct disruption of vessel integrity by radiation. Tissue immunohistochemical staining could not detect elevated global VEGF levels until 48 hours posttreatment; however, localized ischemic VEGF expression was observed at 24 hours posttreatment in these tumors (data not shown). This localized VEGF expression would be expected both to support the survival and to increase the permeability of functioning, refractory tumor vessels imaged by DCE-MRI at this early time point. Constitutive expression of murine VEGF by C6-V cells resulted in higher baseline K_{trans} values, which were not significantly affected either by radiation treatment alone or concurrent radiation and PX-478 (Fig. 6). Delayed refractory tumor growth was seen following combined treatment, indicating that VEGF expression can compensate, albeit not completely, for the pleiotropic antiangiogenic effects of HIF-1 inhibition. Thus, combined ultrasound-MRI imaging confirmed that PX-478 tumor vessel effects are driven by downstream proangiogenic signaling events. Unlike macromolecular MRI contrast agents, small molecular weight Gd-DTPA is currently available for use in patients. Thus, serial Gd-DTPA

DCE-MRI imaging is a potentially promising approach for early assessment of treatment response to PX-478 in the clinical setting.

Adjuvant PX-478 treatment seems roughly equivalent to concurrent treatment for sensitizing C6 and HN5 xenografts to single-fraction radiation, again supporting a model in which HIF-1 inhibition sensitizes tumor cells through indirect microenvironmental effects. Previous studies using genetic knockdown of HIF-1 in HCT-116 and PC-3 xenografts (22) confirm that HIF-1 inhibition instituted either before or following radiation sensitizes tumor vessels to radiation damage. Targeted inhibition of HIF-1 has been confirmed to provide direct antitumor activity in additional preclinical studies (23). The ability of PX-478 to both directly and indirectly radiosensitize tumor cells offers the advantage of addressing multiple microenvironmental niches within tumors. Direct PX-478 effects would sensitize viable hypoxic tumor cell populations, whereas indirect stromal effects would target baseline hypoxic and normoxic tumor regions alike during the later phase of postradiation adaptation. This would support concurrent use of PX-478 with radiation, and our data suggest that concurrent PX-478 treatment with radiation may indeed prove preferable to sequential sequencing, at least in specific tumor types. Concurrent treatment provides more durable inhibition of HIF-1 and VEGF tumor expression in our C6 model (Fig. 5). To explain this, we observed focal regions of refractory HIF-1 and VEGF signaling in tumors adjuvantly treated with PX-478. These regions colocalized to poorly vascularized regions with low $CD105^+$ vessel density tumor, suggesting reduced vascular drug delivery following radiation treatment (data not shown). The logistics of serial multimodality imaging precluded protracted treatment courses with higher cumulative radiation and drug exposures, necessitating limited time periods of tumor growth assessment. Follow-up studies with longer fractionated radiation and drug courses, which recapitulate current clinical treatment strategies, are on-going and will permit exploitation of repetitive perturbations of tumor oxygenation status and stromal function with PX-478. Regardless, the single fraction, higher-dose radiation treatment used in this study with PX-478 remains clinically relevant. High single-dose irradiation yields profound antivascular effects. High-dose radiation induces endothelial cell dysfunction (24) and/or apoptosis (25) and interrupts microvascular blood flow due to luminal collapse and formation of microthrombi (26). Therefore, PX-478 is a promising complement to the antitumor stromal effects of high-dose per fraction therapy, such as stereotactic radiosurgical strategies currently used in the clinic.

HIF-1 knockdown leads to variable effects across cell types and our understanding of the mechanistic roles played by HIF-α family members across individual tumors remains incomplete. Two additional members of the HIF-α family have been identified, designated as HIF-2α and HIF-3α. These proteins heterodimerize with HIF-1β and remain (especially for HIF-3α) understudied. Despite similarities between HIF-1α and HIF-2α, there is little redundancy between the downstream gene regulation and phenotype of these two proteins (27,28). Our own preliminary work suggests that PX-478 also acts a HIF-2 inhibitor[5]; however, we have found HIF-2 to be only weakly expressed in C6 and HN5 cells.

Blouw et al. (29) have shown that HIF blockade can potentially lead to increased vessel co-option in brain parenchyma versus poorly vascularized skin, emphasizing the importance of the host tissue toward defining the clinical effects of HIF-1 blockade. *In situ* spatiotemporal imaging promises to better clarify adaptive whole tumor treatment responses across specific host organs and to permit rational sequencing of radiation and HIF-1–targeted therapy (30). DCE-MRI of low HIF-1–expressing A-549 xenografts refractory to PX-478 indicate that such tumors have low baseline tumor vessel permeability surface area product values

[5]M. Koh, personal communication.

relative to sensitive HT-29 xenografts (13); this suggests that DCE-MRI would be a useful predictive measure of treatment response to PX-478 or other HIF-1–targeted treatments.

In summary, our findings support the central importance of cancer cell HIF-1 signaling to *in vivo* tumor-stromal responses and resistance to radiation treatment. Selective HIF-1 blockade with PX-478 promises durable radiosensitization through inhibition of this mechanism of tumor adaptation, as well as through direct tumor cell sensitization. An important lesson from our findings is that clinical application of targeted HIF-1 radiosensitization strategies will require specific consideration of drug-related microenvironmental mechanisms of action. Preclinical imaging strategies are well suited to guide characterization of such mechanisms and to streamline development of targeted radiosensitization strategies.

Acknowledgments

Grant support: New Program Development Funds and faculty start-up funding from the Department of Experimental Diagnostic Imaging (J. Gelovani and M. Alauddin), NIH grant CA017094 (G. Powis and D. Schwartz), NIH grants CA98920 and CA1019552 (G. Powis), and the Experimental Cancer Imaging Research Program (U24-CA126577) and Cancer Center Support Grant (P30-CA016672) at M. D. Anderson. D. Schwartz received support from the University of Texas Inter-Institutional Biomedical Engineering Program and grant-in-aid funding from Hitachi, Ltd.

References

1. Brizel DM, Scully SP, Harrelson JM, et al. Tumor oxygenation predicts for the likelihood of distant metastases in human soft tissue sarcoma. Cancer Res 1996;56:941–943. [PubMed: 8640781]
2. Hockel M, Schlenger K, Aral B, Mitze M, Schaffer U, Vaupel P. Association between tumor hypoxia and malignant progression in advanced cancer of the uterine cervix. Cancer Res 1996;56:4509–4515. [PubMed: 8813149]
3. Nordsmark M, Overgaard J. A confirmatory prognostic study on oxygenation status and loco-regional control in advanced head and neck squamous cell carcinoma treated by radiation therapy. Radiother Oncol 2000;57:39–43. [PubMed: 11033187]
4. Quintiliani M. Modification of radiation sensitivity: the oxygen effect. Int J Radiat Oncol Biol Phys 1979;5:1069–1076. [PubMed: 389899]
5. Semenza GL. HIF-1: mediator of physiological and pathophysiological responses to hypoxia. J Appl Physiol 2000;88:1474–1480. [PubMed: 10749844]
6. Semenza GL. HIF-1, O(2), and the 3 PHDs: how animal cells signal hypoxia to the nucleus. Cell 2001;107:1–3. [PubMed: 11595178]
7. Powis G, Kirkpatrick L. Hypoxia inducible factor-1α as a cancer drug target. Mol Cancer Ther 2004;3:647–654. [PubMed: 15141023]
8. Semenza GL. Targeting HIF-1 for cancer therapy. Nat Rev Cancer 2003;3:721–732. [PubMed: 13130303]
9. Pugh CW, Ratcliffe PJ. Regulation of angiogenesis by hypoxia: role of the HIF system. Nat Med 2003;9:677–684. [PubMed: 12778166]
10. Belozerov VE, Van Meir EG. Hypoxia inducible factor-1: a novel target for cancer therapy. Anticancer Drugs 2005;16:901–909. [PubMed: 16162966]
11. Koh MY, Spivak-Kroizman T, Venturini S, et al. Molecular mechanisms for the activity of PX-478, an antitumor inhibitor of the hypoxia-inducible factor-1α. Mol Cancer Ther 2008;7:90–100. [PubMed: 18202012]
12. Welsh S, Williams R, Kirkpatrick L, Paine-Murrieta G, Powis G. Antitumor activity and pharmacodynamic properties of PX-478, an inhibitor of hypoxia-inducible factor-1α. Mol Cancer Ther 2004;3:233–244. [PubMed: 15026543]
13. Jordan BF, Runquist M, Raghunand N, et al. Dynamic contrast-enhanced and diffusion MRI show rapid and dramatic changes in tumor microenvironment in response to inhibition of HIF-1α using PX-478. Neoplasia 2005;7:475–485. [PubMed: 15967100]

14. Wen B, Burgman P, Zanzonico P, et al. A preclinical model for noninvasive imaging of hypoxia-induced gene expression; comparison with an exogenous marker of tumor hypoxia. Eur J Nucl Med Mol Imaging 2004;31:1530–1538. [PubMed: 15378285]
15. Serganova I, Doubrovin M, Vider J, et al. Molecular imaging of temporal dynamics and spatial heterogeneity of hypoxia-inducible factor-1 signal transduction activity in tumors in living mice. Cancer Res 2004;64:6101–6108. [PubMed: 15342393]
16. Alauddin MM, Conti PS, Fissekis JD. A general synthesis of [18F] labeled 2′-deoxy-2′-fluoro-1-β-d-arabinofuranosyluracil nucleosides. J Labelled Comp Radiopharm 2003;46:285–289.
17. Nordsmark M, Alsner J, Keller J, et al. Hypoxia in human soft tissue sarcomas: adverse impact on survival and no association with p53 mutations. Br J Cancer 2001;84:1070–1075. [PubMed: 11308256]
18. Joyce JA. Therapeutic targeting of the tumor microenvironment. Cancer Cell 2005;7:513–520. [PubMed: 15950901]
19. Ceelen W, Smeets P, Backes W, et al. Noninvasive monitoring of radiotherapy-induced microvascular changes using dynamic contrast enhanced magnetic resonance imaging (DCE-MRI) in a colorectal tumor model. Int J Radiat Oncol Biol Phys 2006;64:1188–1196. [PubMed: 16457965]
20. Kobayashi H, Reijnders K, English S, et al. Application of a macromolecular contrast agent for detection of alterations of tumor vessel permeability induced by radiation. Clin Cancer Res 2004;10:7712–7720. [PubMed: 15570005]
21. Crokart N, Jordan BF, Baudelet C, et al. Early reoxygenation in tumors after irradiation: determining factors and consequences for radiotherapy regimens using daily multiple fractions. Int J Radiat Oncol Biol Phys 2005;63:901–910. [PubMed: 16199320]
22. Moeller BJ, Dreher MR, Rabbani ZN, et al. Pleiotropic effects of HIF-1 blockade on tumor radiosensitivity. Cancer Cell 2005;8:99–110. [PubMed: 16098463]
23. Kung AL, Wang S, Klco JM, Kaelin WG, Livingston DM. Suppression of tumor growth through disruption of hypoxia-inducible transcription. Nat Med 2000;6:1335–1340. [PubMed: 11100117]
24. Garcia-Barros M, Paris F, Cordon-Cardo C, et al. Tumor response to radiotherapy regulated by endothelial cell apoptosis. Science 2003;300:1155–1159. [PubMed: 12750523]
25. Paris F, Fuks Z, Kang A, et al. Endothelial apoptosis as the primary lesion initiating intestinal radiation damage in mice. Science 2001;293:293–297. [PubMed: 11452123]
26. Guelinckx PJ, Boeckx WD, Fossion E, Gruwez JA. Scanning electron microscopy of irradiated recipient blood vessels in head and neck free flaps. Plast Reconstr Surg 1984;74:217–226. [PubMed: 6463146]
27. Wenger RH. Cellular adaptation to hypoxia: O_2-sensing protein hydroxylases, hypoxia-inducible transcription factors, and O_2-regulated gene expression. FASEB J 2002;16:1151–1162. [PubMed: 12153983]
28. Wang V, Davis DA, Haque M, Huang LE, Yarchoan R. Differential gene up-regulation by hypoxia-inducible factor-1α and hypoxia-inducible factor-2α in HEK293T cells. Cancer Res 2005;65:3299–3306. [PubMed: 15833863]
29. Blouw B, Song H, Tihan T, et al. The hypoxic response of tumors is dependent on their microenvironment. Cancer Cell 2003;4:133–146. [PubMed: 12957288]
30. Tatum JL, Kelloff GJ, Gillies RJ, et al. Hypoxia: importance in tumor biology, noninvasive measurement by imaging, and value of its measurement in the management of cancer therapy. Int J Radiat Biol 2006;82:699–757. [PubMed: 17118889]

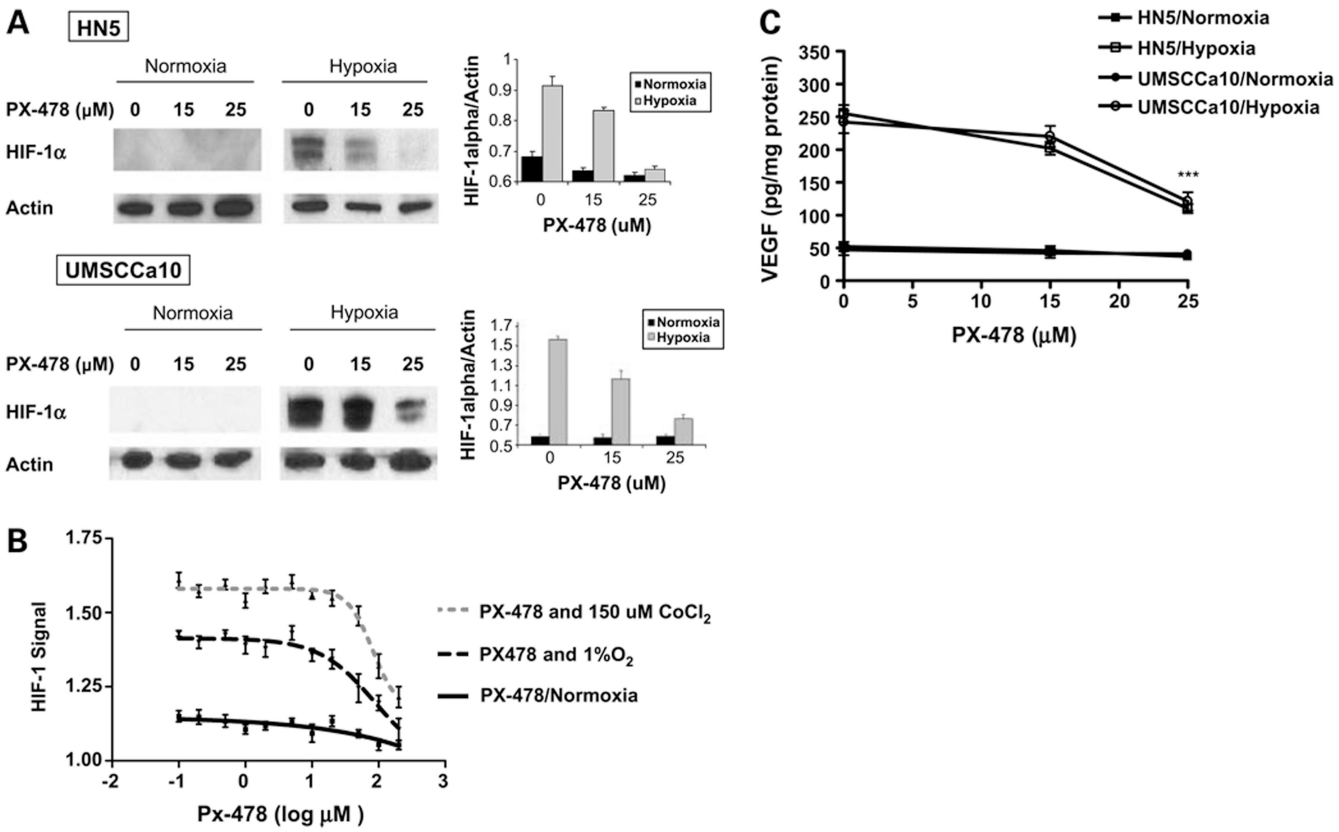

Figure 1.

PX-478 inhibits hypoxic HIF-1 protein expression and signaling activity in a dose-dependent manner. **A,** HN5 and UMSCCA10 cells were treated with PX-478 at indicated concentrations for 24 h under normoxic (air, 5% CO_2) or hypoxic (1% O_2, 5%CO_2, 94% N_2) conditions. Western blots were quantified by densitometry relative to actin. *Columns*, normalized mean absorbance values plotted from triplicate experiments; *bars*, SE. **B,** C6 HIF-1 reporter cells were created via stable transfection with a bifunctional genetic reporter consisting of HSV-tk and GFP under transcriptional control of the hypoxia response element (HRE-tk/eGFP-cmvRed 2XPRT). Cells were treated with PX-478 at concentrations ranging from 0.1 to 200 μmol/L, with or without concurrent 150 μmol/L $CoCl_2$ chemical stimulation of HIF-1 signaling for 24 h. Experiments were repeated in hypoxic conditions, with cells incubated at 1% O_2 (hypoxia, via chamber) for 24 h and then treated with PX-478 at equivalent concentrations for 24 h. HIF-1–dependent GFP signal normalized to beacon RFP signal was measured in quadruplicate. *Points*, mean; *bars*, SE. **C,** VEGF protein per milligram of total secreted protein measured by ELISA in supernatant medium from HN5 and UMSCCa10 cells cultured in normoxic or 1% O_2 (24 h, via chamber) conditions, with or without 24-h treatment with indicated concentrations of PX-478. *Points*, mean from three separate experiments; *bars*, SD. ***, $P < 0.001$.

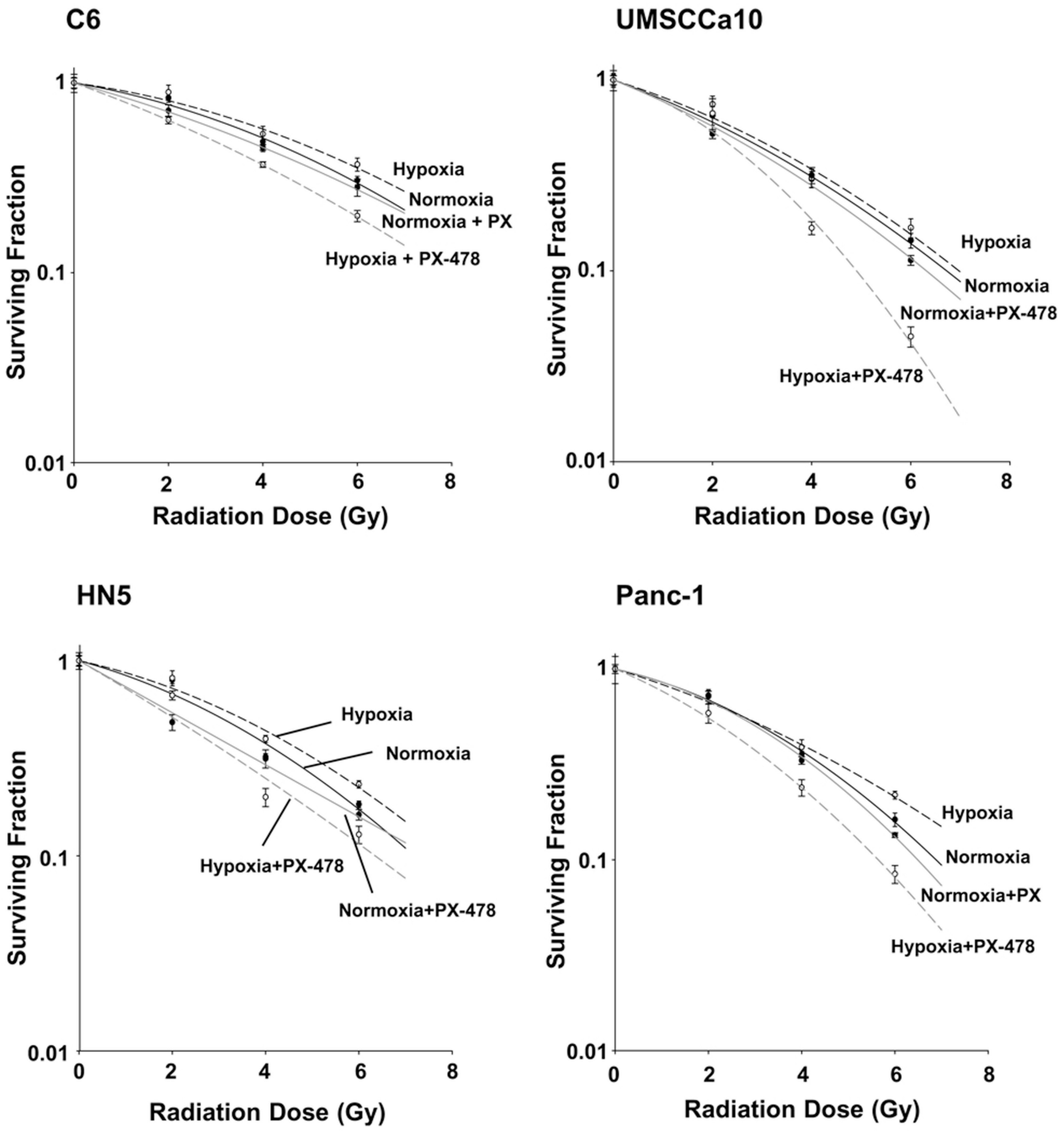

Figure 2.

PX-478 directly radiosensitizes tumor cells *in vitro*. C6, HN5, Panc-1, and UMSCCA10 cells were grown in monolayer cultures for 24 h under normoxic (air, 5% CO_2) or hypoxic (1% O_2, 5% CO_2, 94% N_2) conditions. Cells were either left as untreated controls or treated with 25 μmol/L PX-478 for 24 h with atmospheric conditions held constant. Cells were irradiated with increasing doses (2, 4, or 6 Gy) of radiation with atmospheric treatment conditions maintained. The cells were assayed for colony-forming ability by replating at specified numbers into six-well plates in a drug-free medium. The cells were immediately plated after irradiation, maintained for 12 d in normoxic conditions to allow for repopulation of surviving clones, stained, and counted. Clonogenic survival curves were constructed from

at least three independent experiments by fitting the average survival levels using least squares regression by the linear quadratic model. Normoxia, control (——); hypoxia, control (------); normoxia, PX-478 treated (——); hypoxia, PX-478 treated (------).

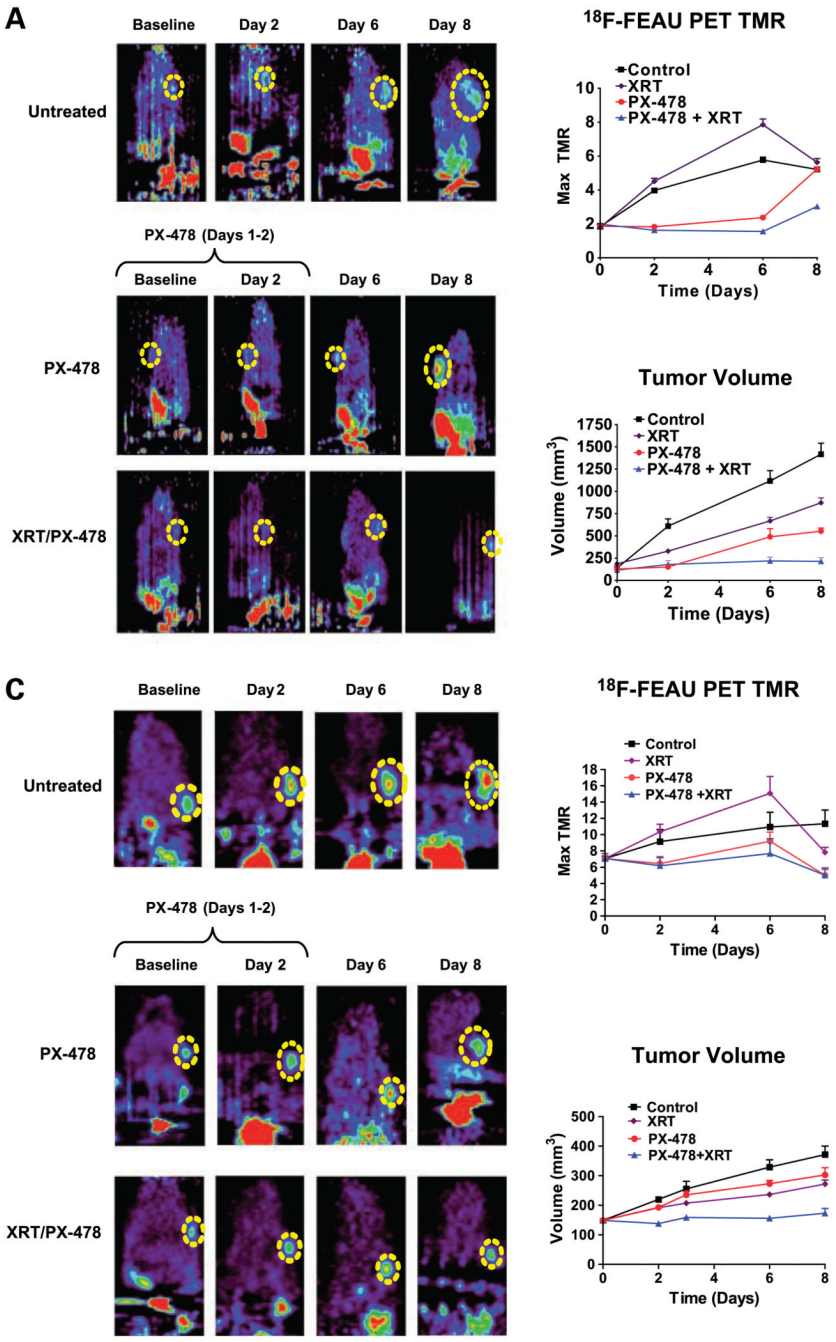

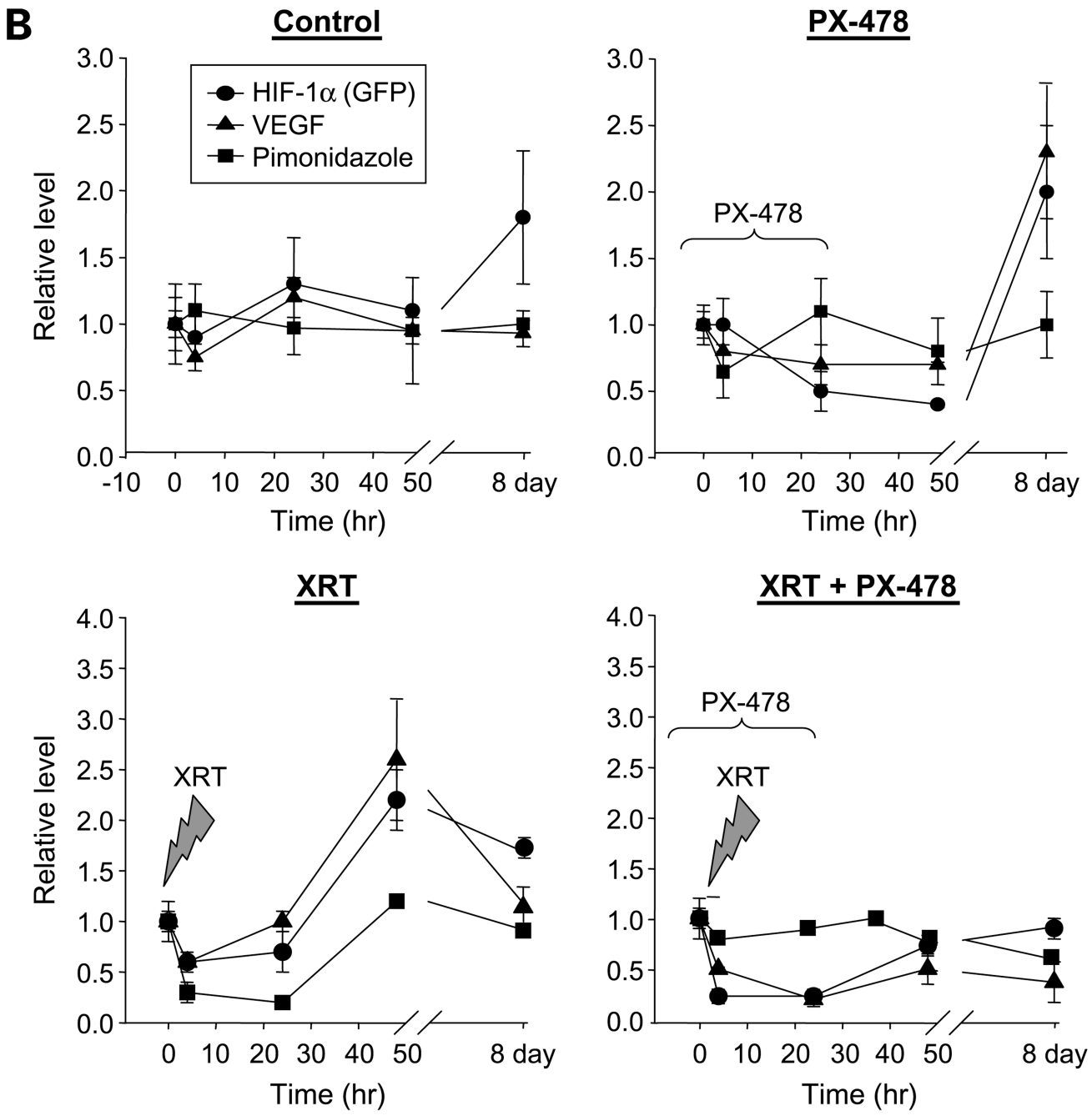

Figure 3.

PX-478 inhibits tumor HIF-1 signaling *in vivo* and markedly enhances growth delay in C6 and HN5 xenografted tumors following single-fraction radiation. **A,** ^{18}F-FEAU PET imaging of C6 reporter xenografts (n = 8–10 in each study cohort) treated with 30 mg/kg PX-478 with or without 8 Gy single-fraction irradiation (*XRT*). Each series of images was obtained from the same animal at indicated time points. PX-478 was administered on days 1 and 2 of the time course, after baseline images had been obtained. *Dashed yellow circle,* location of each tumor on PET images. Animals are oriented with head at the top of each image; nonspecific bladder/kidney signal is seen below due to urinary excretion of ^{18}F-FEAU. *Points,* mean values for maximum TMR of ^{18}F-FEAU accumulation; *bars,* SE (*top*

right). *Points,* mean values for tumor volumes across time; *bars,* SE (*bottom right*). **B,** C6 reporter xenograft tissue was harvested at indicated time points for immunohistochemical staining for HIF-1–dependent GFP expression (●), downstream VEGF expression (▲), and hypoxia-dependent retention of pimonidazole (■). *Points,* mean values (n = 4 tumors × 5 tissue sections) of expression levels normalized to baseline values; *bars,* SE. **C,** ^{18}F-FEAU PET imaging of HN5 reporter xenografts (n = 6 per cohort) treated with 30 mg/kg PX-478 with or without 8 Gy single-fraction irradiation. *Points,* mean values for maximum TMR and tumor volumes, plotted as in **A**; *bars,* SE.

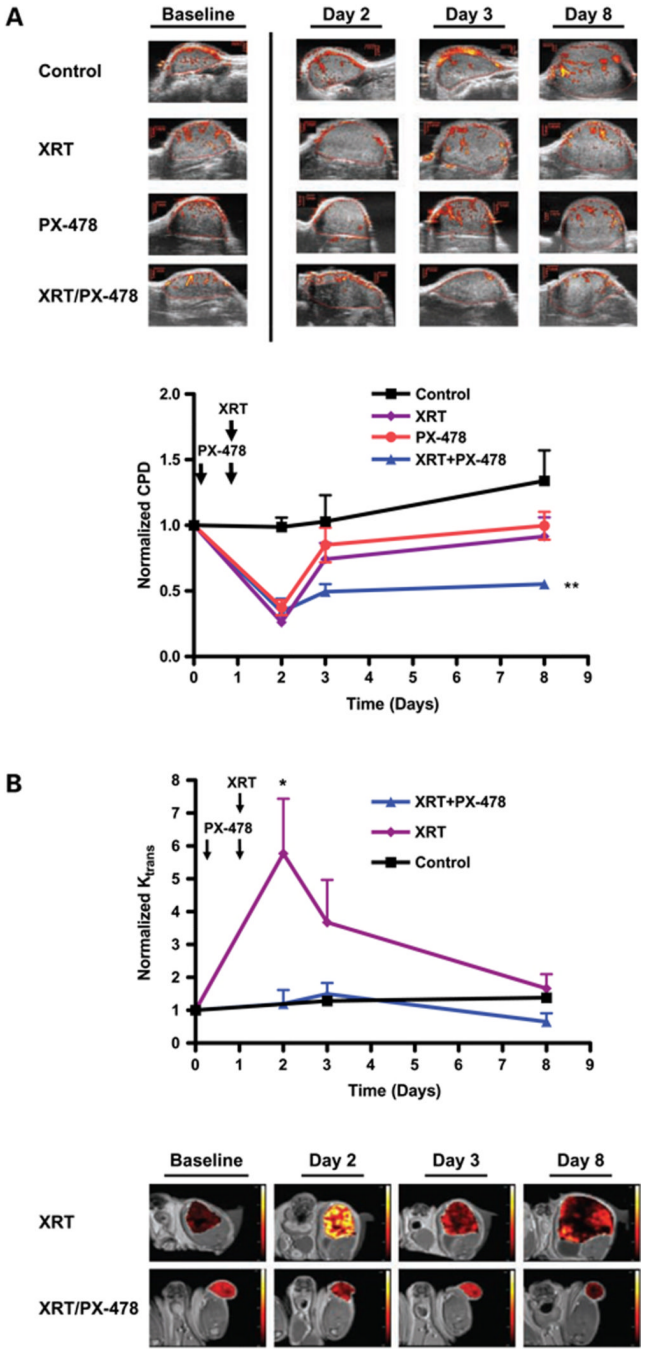

Figure 4.

Durable inhibition of posttreatment tumor stromal recovery in C6 tumor xenografts following combined PX-478 and radiation. **A,** power Doppler ultrasound measurements of tumor blood flow at noted time points following treatment with 8 Gy alone, 30 mg/kg PX-478 × 2 d, or combined treatment (n = 6 per cohort). Timing of respective treatments following baseline imaging (day 0) are noted, with radiation administered on day 1 and PX-478 administered after baseline imaging on days 0 and 1. For combined radiation and PX-478 treatment, animals received the first dose of PX-478 the day before irradiation and the second dose 4 h before irradiation. Vascular area in tumor was calculated by color pixel density (*CPD*) for each tumor, defined as the ratio of the number of color pixels within the

tumor to total number of pixels. *Points*, mean values for tumor color pixel density; *bars*, SE. Results for combined PX-478 and radiation treatment at day 7 were compared with baseline values; **, $P < 0.005$. **B,** serial DCE-MRI K_{trans} mapping for C6 xenografts treated with 8 Gy with or without 30 mg/kg PX-478 × 2 d ($n = 5$ per cohort). Timing and sequencing of treatments were kept consistent with those described above. *Points*, mean tumor K_{trans} values; *bars*, SE. Results for radiation treatment alone at day 2 were compared with baseline values; *, $P < 0.05$.

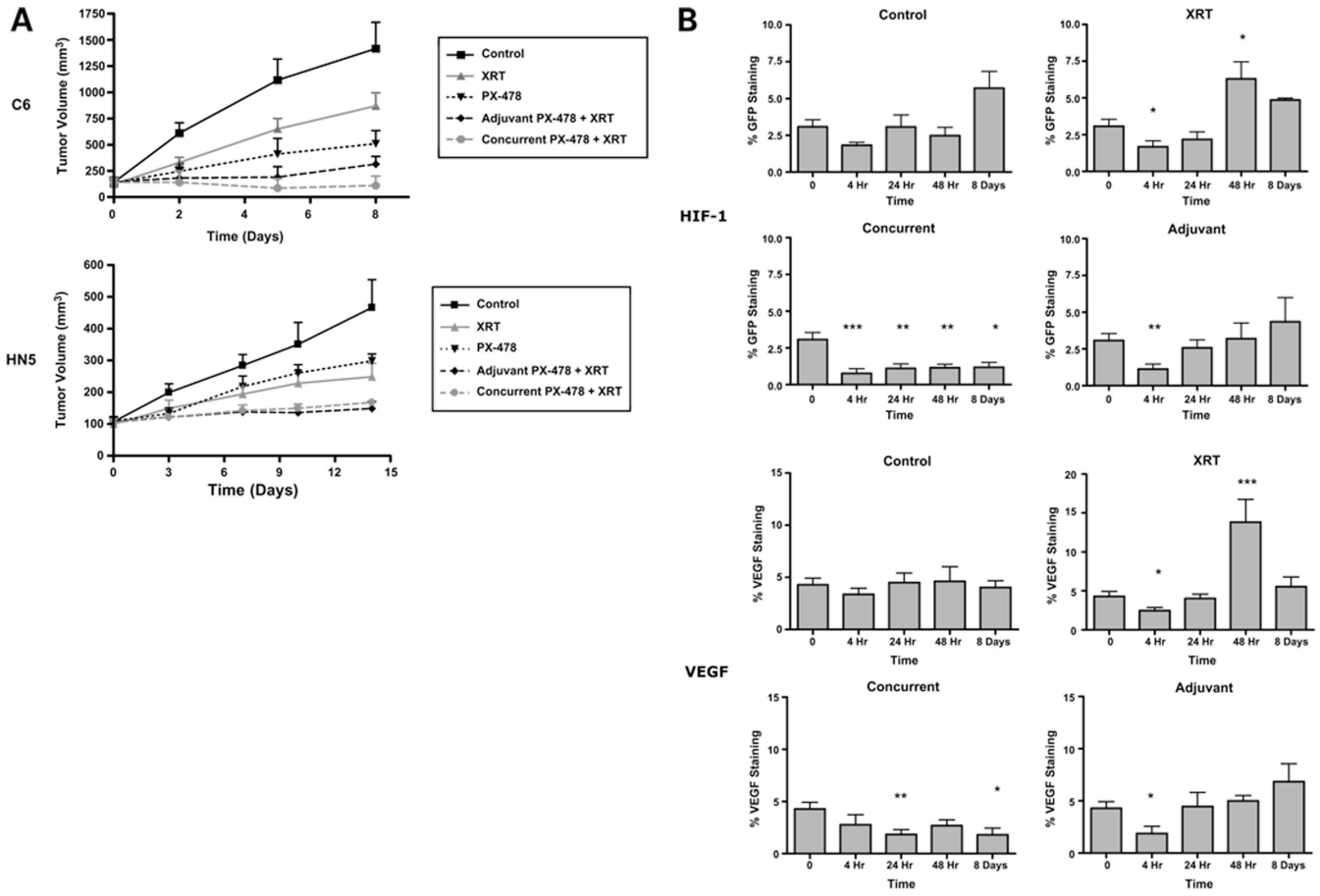

Figure 5.

Sequencing of PX-478 with radiation treatment of C6 and HN5 xenografts shows that *in vivo* PX-478 radiosensitization is mediated through effects on tumor stromal adaptation. C6 (n = 8) and HN5 (n = 10) xenograft cohorts were treated with 8 Gy alone, a 2-d course of 30 mg/kg p.o. PX-478 alone, or one of two combined treatment sequences: concurrent, with PX-478 given the day before and 4 h before irradiation, or adjuvant, with a 2-d course of PX-478 initiated the day following irradiation. **A,** tumor growth curves. *Points*, mean volumes; *bars*, SE. **B,** serial quantification of %HIF-1/VEGF staining of C6 xenograft tissue (n = 4 tumors × 5 tissue sections) treated with 8 Gy alone or with the above noted concurrent or adjuvant 30 mg/kg PX-478 treatment. Time 0 refers to pooled pretreatment baseline values. Subsequent time points refer to number of hours following administration of radiation. Statistical comparisons of results at each time point are with baseline findings. *Columns*, mean; *bars*, SE. *, $P < 0.05$; **, $P < 0.005$, ***, $P < 0.001$.

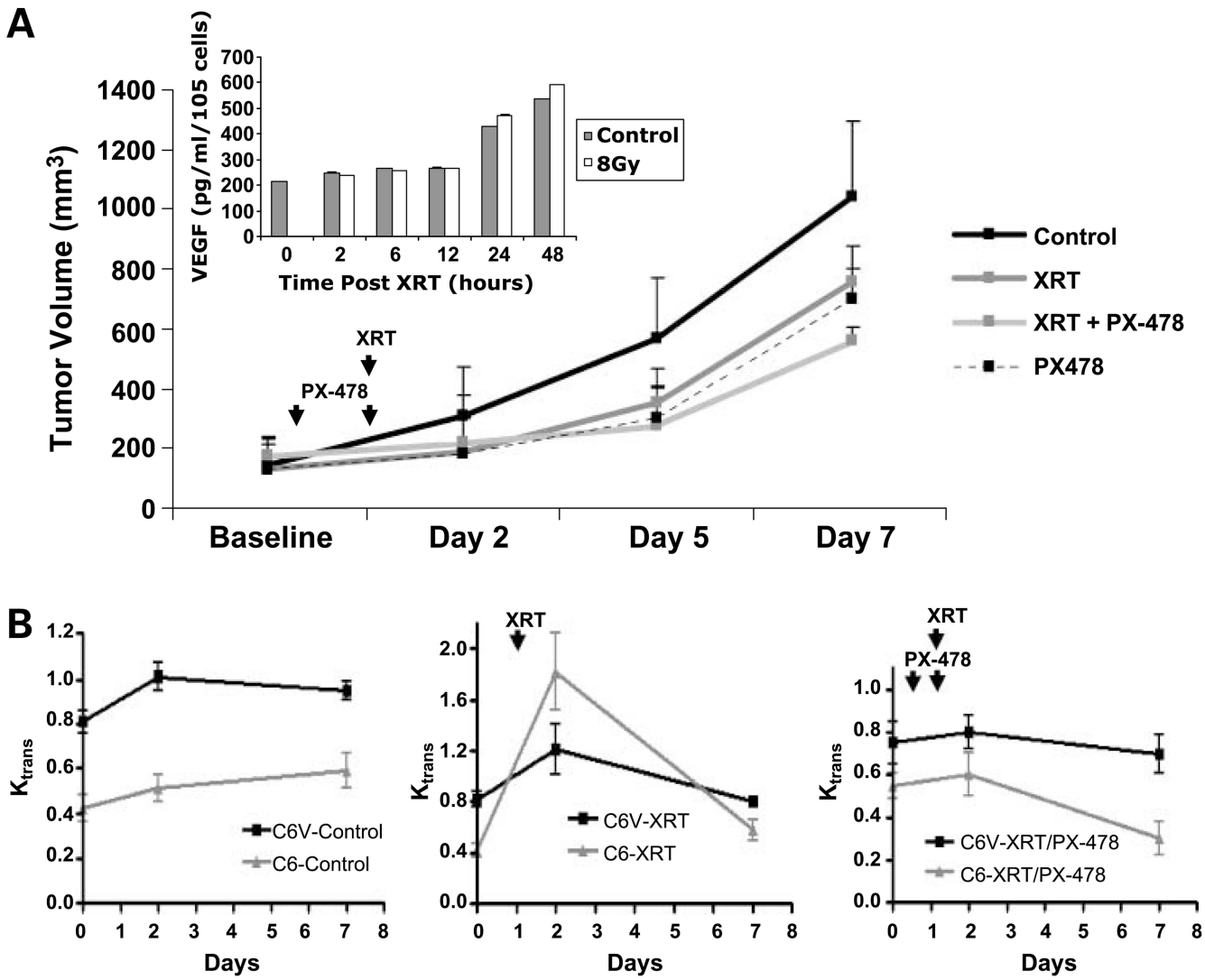

Figure 6.

Downstream angiogenic signaling mediates *in vivo* PX-478 radiosensitization. C6 cells were stably transfected with a constitutive murine VEGF expression construct (C6-V) to provide uninterrupted proangiogenic signaling to host mouse stroma. C6-V xenograft cohorts ($n = 6$) were treated with 8 Gy with or without a 2-d course of 30 mg/kg p.o. PX-478 given the day before and 4 h before irradiation. **A,** tumor growth curves. *Points*, mean volumes; *bars*, SE. *Inset*, secreted VEGF protein in C6-V supernatant medium quantified by ELISA at specified time points following treatment with 8 Gy. **B,** serial DCE-MRI K_{trans} mapping for C6-V xenografts treated with 8 Gy with or without 30 mg/kg PX-478 × 2 d ($n = 5$ per cohort). Timing of respective radiation and drug treatments following baseline imaging at day 0 is as annotated. *Points*, mean tumor K_{trans} values; *bars*, SE.